ACS central science

Research Article

http://pubs.acs.org/journal/acscii

In Situ Electrochemical Oxidation Tuning of Transition Metal Disulfides to Oxides for Enhanced Water Oxidation

Wei Chen,[†] Haotian Wang,[‡] Yuzhang Li,[†] Yayuan Liu,[†] Jie Sun,[†] Sanghan Lee,[†] Jang-Soo Lee,[†] and Yi Cui*[,†,§]

[†]Department of Materials Science and Engineering and [‡]Department of Applied Physics, Stanford University, Stanford, California 94305, United States

[§]Stanford Institute for Materials and Energy Sciences, SLAC National Accelerator Laboratory, Menlo Park, California 94025, United States

Supporting Information

ABSTRACT: The development of catalysts with earth-abundant elements for efficient oxygen evolution reactions is of paramount significance for clean and sustainable energy storage and conversion devices. Our group demonstrated recently that the electrochemical tuning of catalysts via lithium insertion and extraction has emerged as a powerful approach to improve catalytic activity. Here we report a novel in situ electrochemical oxidation tuning approach to develop a series of binary, ternary, and quaternary transition metal (e.g., Co, Ni, Fe) oxides from their corresponding sulfides as highly active catalysts for much enhanced water oxidation. The electrochemically tuned cobalt−nickel−iron oxides grown directly on the three-dimensional carbon fiber electrodes exhibit a low overpotential of 232 mV at current density of 10 mA cm^{-2}, small Tafel slope of 37.6 mV dec^{-1}, and exceptional long-term stability of electrolysis for over 100 h in 1 M KOH alkaline medium, superior to most non-noble oxygen evolution catalysts reported so far. The materials evolution associated with the electrochemical oxidation tuning is systematically investigated by various characterizations, manifesting that the improved activities are attributed to the significant grain size reduction and increase of surface area and electroactive sites. This work provides a promising strategy to develop electrocatalysts for large-scale water-splitting systems and many other applications.

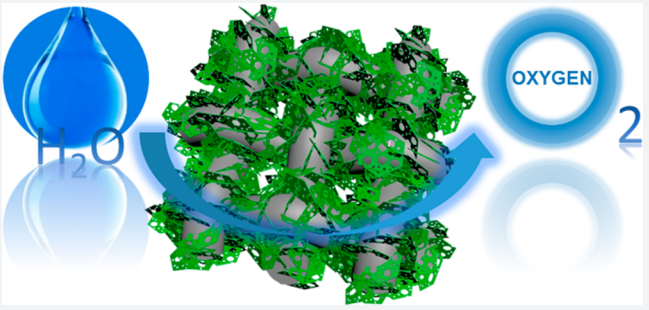

Water oxidation catalysts play a pivotal role in the sustainable and efficient energy conversion and storage systems, such as water electrolyzers, solar water-splitting devices, and rechargeable metal−air batteries.[1−5] Oxygen evolution reaction (OER) catalysts enable the generation of oxygen by means of electrochemical water oxidation that is considered to be kinetically sluggish.[6,7] Efficient electrocatalysts are of great significance to facilitate the oxidation process in terms of reducing the overpotential and improving the conversion efficiency. In reality, two fundamental obstacles need to be overcome in the development of active electrocatalysts for efficient water oxidation in large scale: the high overpotentials and the poor stability of the OER catalysts.[8] While some highly active, precious metal oxides such as IrO_2 and RuO_2 are demonstrated to be the state-of-the-art OER catalysts, they suffer from high cost and scarcity of the precious metals, which would seriously impede their widespread applications.[9−11] In recent years, substantial efforts have been devoted to developing earth-abundant, cost-effective OER catalysts, in which transition metal oxides and hydroxides, chalcogenides, phosphates, and perovskites are extensively investigated.[12−25] Particularly, the transition metal oxides and hydroxides have demonstrated some of the most exciting electrocatalytic properties for low-cost and durable OER catalysts, even outperforming that of the precious metal oxides.[26−28] Yet further improvement of the OER performance of the transition metal oxides has become challenging.

There exist multiple approaches to further improve the OER activity of the transition metal oxides. One effective approach is to synthesize complex metal oxides, where the mixed metal oxides show OER performance superior to that of single metal oxides.[8,29−32] For example, Louie et al. reported that a Ni−Fe oxide thin film exhibited OER activity much higher than that of Ni oxide and Fe oxide films.[32] Burke et al. revealed that the intrinsic OER activity of Co−Fe oxyhydroxide is about 2 orders higher than that of CoOOH.[31] Another attractive solution is to fabricate nanostructured ultrathin nanosheets or ultrasmall nanoparticles of transition metal oxides, so as to increase the active catalytic sites for enhanced OER properties.[19,33,34] As reported by Song et al., the exfoliated single layer nanosheets of the layered double hydroxides exhibited higher OER activity than that of the corresponding bulk counterparts.[33] The ultrasmall nanoparticles of NiO with size between 2.5 and 5 nm

Received: June 7, 2015
Published: July 15, 2015

DOI: 10.1021/acscentsci.5b00227
ACS Cent. Sci. 2015, 1, 244−251

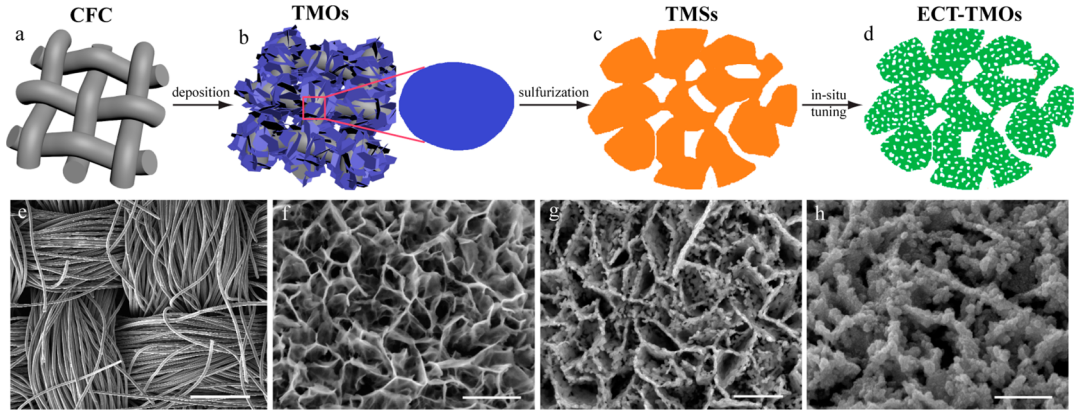

Figure 1. Schematic illustration of the synthesis process of ECT-TMOs and their corresponding morphology. (a) Carbon fiber cloth substrate. (b) Pristine TMOs coated on CFC by the one-step electrochemical deposition. (c) TMSs obtained by the sulfurization treatment of the pristine TMOs. (d) ECT-TMOs formed by the in situ electrochemical oxidation tuning of TMSs. (e–h) SEM images of CFC, CoO, CoS_2, and ECT-CoO respectively. Scale bars: (e) 200 μm; (f–h) 500 nm.

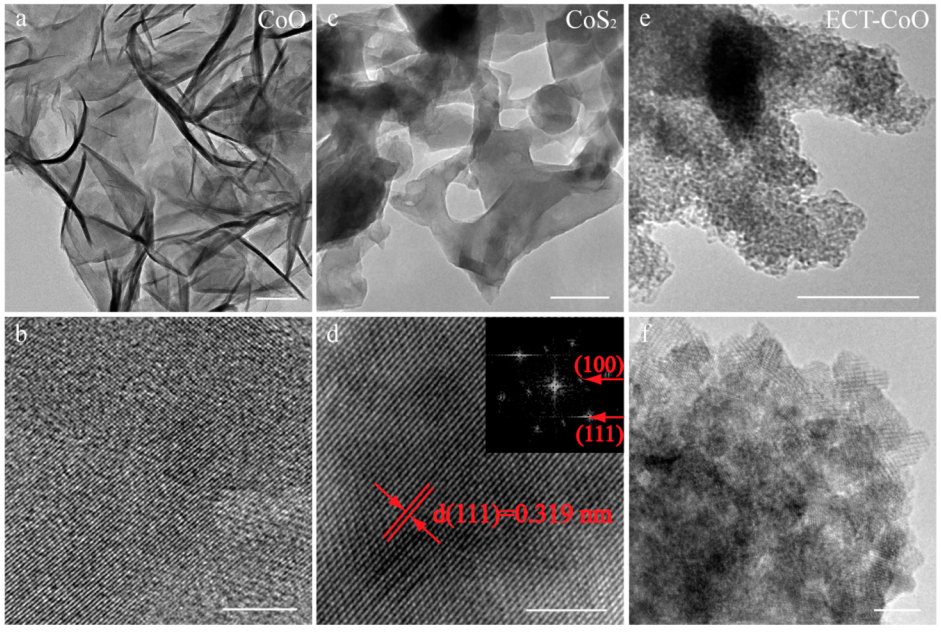

Figure 2. TEM characterization of CoO/CoS_2/ECT-CoO: (a, b) pristine CoO, (c, d) CoS_2, and (e, f) ECT-CoO, respectively. Scale bars: (a) 100 nm; (c, e) 50 nm; (b, d, f) 5 nm.

also showed good performance for electrochemical water oxidation.[34] Moreover, one promising strategy on improving the OER performance is to make poor crystalline or amorphous transition metal oxides that possess more defects or vacancies serving as active sites to efficiently catalyze the water oxidation reactions.[22,35−38] For example, the Nocera group reported amorphous cobalt phosphate and nickel borate as excellent OER catalysts in neutral water.[22,35] The Berlinguette group introduced a photochemical method to produce a series of amorphous transition metal oxides that operated superior to that of crystalline oxides.[36] Recently, our group has developed a general methodology of the electrochemical tuning by lithium insertion and extraction for both hydrogen and oxygen evolution reactions.[39−43] In this method, lithium insertion and extraction are used to tune the electronic structure, conductivity, defect, grain size and boundary, and surface area of catalysts, resulting in significant improvement of catalytic activity. Built on these understandings, we hypothesize that there exist other electrochemical and chemical tuning methods, which can significantly improve activity of catalysts with similar chemical compositions.

In this work, we report a novel in situ electrochemical oxidation tuning approach for the synthesis of nanoporous transition metal oxides (TMOs) as OER catalysts with significantly enhanced activity. The materials synthesis process is schematically illustrated in Figure 1. First, we deposited TMOs electrochemically onto three-dimensional (3D) conductive carbon fiber cloth (CFC) (Figure 1a,b). The interwoven CFC was chosen as the substrate for the integrated electrode due to its excellent electrical conductivity, 3D macroporous structure, and stable electrochemical features (Figure 1e). Second, the TMOs deposited on CFC were converted to transition metal sulfides (TMSs) by a sulfurization treatment at a temperature of 500 °C (Figure 1c, see Experimental Section in the Supporting Information for details). Finally, the in situ electrochemical tuning was achieved when the TMSs were electrochemically oxidized in alkaline electrolyte at room temperature, transforming them back to

DOI: 10.1021/acscentsci.5b00227
ACS Cent. Sci. 2015, 1, 244−251

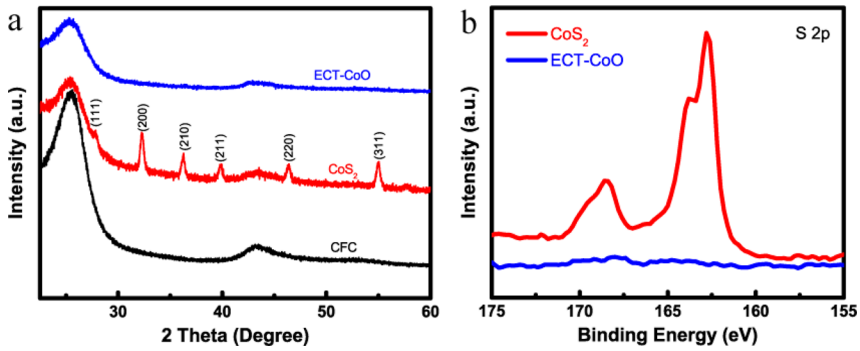

Figure 3. XRD and XPS of ECT-CoO. (a) XRD of CoS_2 and ECT-CoO. (b) The XPS S 2p peaks of CoS_2 and ECT-CoO.

TMOs, henceforth referred to as ECT-TMOs, with significantly different characteristics from the pristine TMOs (Figure 1d). During this whole synthesis process, chemical/electrochemical transformations take place three times and afford the opportunity to tune the catalysts. Small grains and pores are expected to be created when a TMO is converted into a TMS by the high temperature sulfurization treatment. The even smaller grains and pores would be produced when the TMS is electrochemically oxidized back to TMO. The room temperature condition of electrochemical tuning is expected to be important since this prevents the thermal annealing and diffusion to grow large grains. Using CoO as an example, we confirm such a morphology evolution when CoO is sulfurized to CoS_2 and further electrochemically oxidized back to CoO (ECT-CoO). This process is labeled as CoO/CoS_2/ECT-CoO. Scanning electron microscopy (SEM) image shows that the as deposited CoO has nanosheet morphology standing up on the carbon fiber (Figure 1f). The CoS_2 nanosheets inherit the overall morphology of their oxide counterparts (Figure S1a,b) although they exhibit porous microstructures due to the significant atomic diffusion and grain growth during displacement of oxygen by sulfur at high temperature (Figure 1g). The in situ electrochemical oxidation changes the morphology significantly by breaking the materials into many interconnected smaller grains of ECT-CoO (Figure 1h), thereby creating numerous nanopores on the nanosheets of ECT-CoO.

Transmission electron microscopy (TEM) images further confirm the morphology and microstructure evolution in the CoO/CoS_2/ECT-CoO process. As shown in Figure 2a, the pristine CoO has an interconnected nanosheet morphology with smooth surface characteristic. The pristine CoO nanosheets consist of some large grains with sizes greater than 10 nm (Figure 2b). The CoS_2 nanosheets have porous nanostructures with a number of mesopores generated by the sulfurization treatment of the pristine CoO (Figure 2c), consistent with the observation by SEM in Figure 1g. The high resolution transmission electron microscopy (HRTEM) image in Figure 2d shows a highly crystalline characteristic of CoS_2. The crystalline lattice fringe corresponds to the atomic plane of (111) of CoS_2, which is confirmed by its fast Fourier transform (FFT). In contrast, the ECT-CoO exhibits a nanoporous feature with lots of micropores formed on the nanosheets (Figure 2e), drastically distinguished from the rather smooth surface of CoS_2 (Figure 2c) or the pristine CoO (Figure 2a). The HRTEM image further reveals that the ECT-CoO is composed of tiny nanoparticles with grain sizes smaller than 5 nm (Figure 2f). These nanoparticles show weak crystallinity and different grain orientations that interconnect with each other. The ECT-CoO nanosheets therefore demonstrate poor crystallinity but highly porous characteristics, indicating that the in situ electrochemical oxidation tuning process has great impact on the alternation of crystallinity, defects, grain boundaries, and porosity of the materials.

Moreover, X-ray diffraction (XRD), X-ray photoelectron spectroscopy (XPS), and inductively coupled plasma spectrometry (ICP) were carried out to further reveal the evolution of the CoO/CoS_2/ECT-CoO process. As shown in Figure 3a, CoS_2 has a highly crystalline pattern that is well indexed to CoS_2 with cubic structure (PDF no. 04-003-2292), whereas the ECT-CoO demonstrates nearly amorphous or very poor crystalline features, consistent with the observation by TEM (Figure 2c–f). The disappearance of sulfur characteristic peaks in ECT-CoO observed by XPS illustrates the complete transformation of sulfide to oxide by the in situ electrochemical tuning (Figure 3b). This is further confirmed by the ICP-MS and OES elemental analysis of the ECT-CoO, demonstrating the Co/S molar ratio of ~1000:1. As a comparison, the S 2p characteristic peak of CoS_2 at binding energy of 162.8 eV is attributed to the S $2p_{3/2}$ core level that is typical of metal–sulfur bonds and agrees well with the literature.[44,45] The peak located at 168.6 eV corresponds to the surface sulfur with high oxidation state.[46] Regarding the oxidation state of the transition metal, it is observed in Co 2p spectra of CoS_2 and ECT-CoO that the Co peaks shifted to higher binding energy after the in situ electrochemical oxidation tuning, indicating its increased oxidation state (Figure S2). The intensive Co $2p_{3/2}$ peak of the ECT-CoO located at binding energy of 780.2 eV can be indexed to CoOOH, demonstrating that the electrochemical oxidation tuning approach is capable of both sulfur and transition metal oxidation.[47,48] The increased oxidation state of transition metal with higher valence is believed to facilitate the multielectron transportation process involved in water oxidation, which contributes to highly active OER catalysts with better performance.[49,50] In contrast, the pristine CoO that underwent the in situ electrochemical oxidation tuning process shows no change in the crystal phase and composition with good morphology retention (Figure S3).

In addition to CoO, our methodology can be used as a general one to produce a whole family of TMOs. For example, we have also synthesized ternary $Co_{0.5}Fe_{0.5}O$/$Co_{0.5}Fe_{0.5}S_2$/ECT-$Co_{0.5}Fe_{0.5}O$ and quaternary $Co_{0.37}Ni_{0.26}Fe_{0.37}O$/$Co_{0.37}Ni_{0.26}Fe_{0.37}S_2$/ECT-$Co_{0.37}Ni_{0.26}Fe_{0.37}O$ by the same in situ electrochemical oxidation tuning approach. Similar structures of the nanosheets on the 3D porous electrodes were also observed in the ternary $Co_{0.5}Fe_{0.5}O$/$Co_{0.5}Fe_{0.5}S_2$ (Figure S4a,b) and the quaternary $Co_{0.37}Ni_{0.26}Fe_{0.37}S_2$/

DOI: 10.1021/acscentsci.5b00227
ACS Cent. Sci. 2015, 1, 244–251

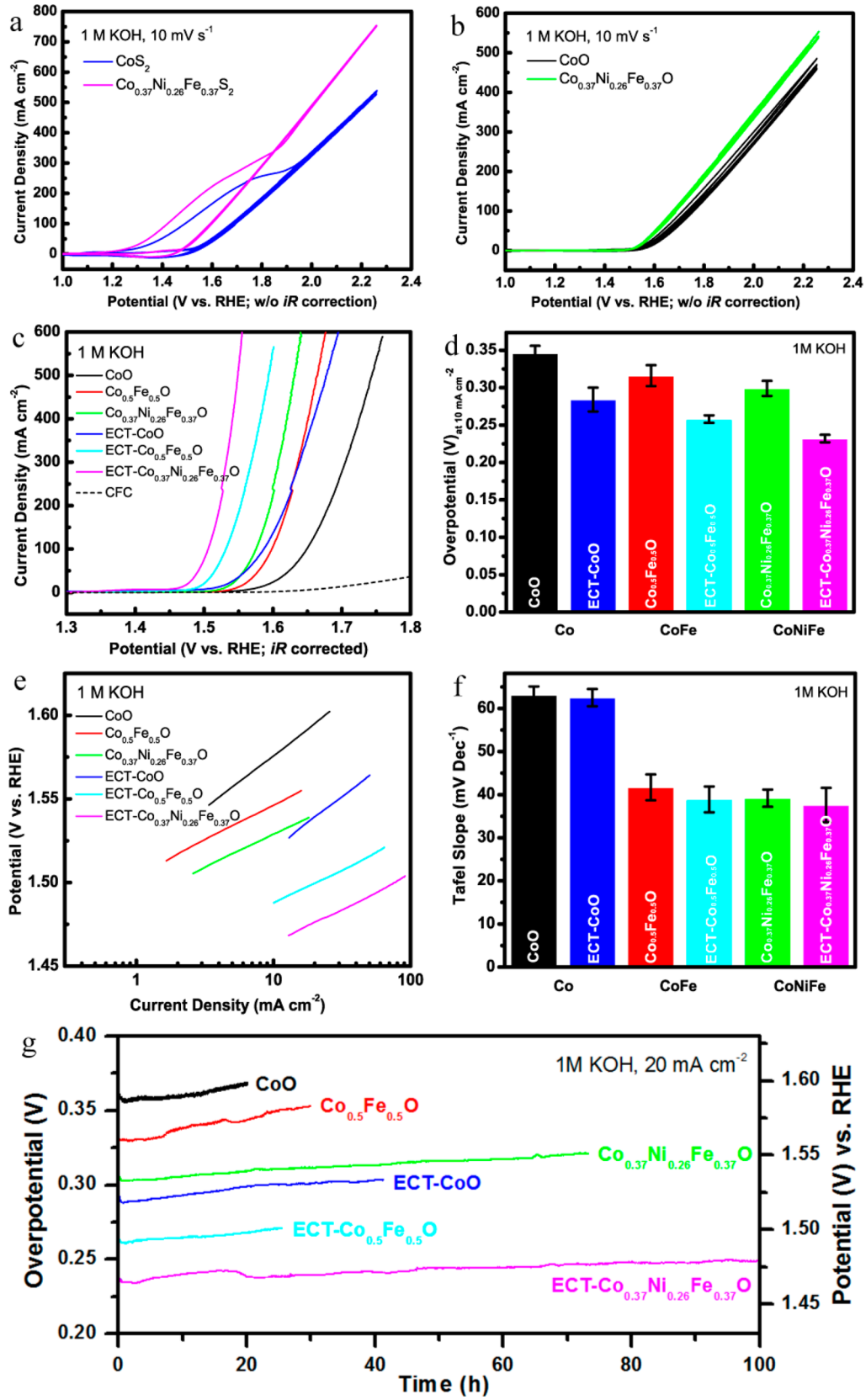

Figure 4. Electrochemical performance of TMOs and ECT-TMOs in alkaline 1 M KOH solution. The first three cyclic voltammetry curves of (a) CoS_2 and $Co_{0.37}Ni_{0.26}Fe_{0.37}S_2$ and (b) pristine CoO and $Co_{0.37}Ni_{0.26}Fe_{0.37}O$, respectively. The curves were not applied to *iR* correction. (c) Polarization curves and (e) Tafel plots of pristine TMOs and ECT-TMOs as comparison, respectively. The curves were *iR* corrected. Summary of (d) overpotential at 10 mA cm^{-2} and (f) Tafel slope of pristine TMOs and ECT-TMOs, respectively. (g) Long-term chronopotentiometric stability behaviors of the pristine TMOs and ECT-TMOs under constant current density of 20 mA cm^{-2}.

DOI: 10.1021/acscentsci.5b00227
ACS Cent. Sci. 2015, 1, 244−251

$Co_{0.37}Ni_{0.26}Fe_{0.37}S_2$ systems (Figure S4c,d), indicating the feasibility of the in situ electrochemical tuning approach for the preparation of a wide range of nanoporous TMOs. The incorporation of Ni and Fe into CoO is achieved by partial substitution of Co with Ni and Fe in the electrochemical codeposition step, attributed to the very close lattice parameters among Co, Ni, and Fe. This is a common approach that was adopted to synthesize complex metal oxides and sulfides as reported previously.[45,S1] It is noted that the composition of the complex TMOs is tunable by controlling different ratios among the transitional metals, however, we focus in the present study on investigating the TMOs with equal concentrations of different transition metals in their preparation solutions. Nevertheless, the obtained TMOs that contain nickel show a little lower ratio than its feeding ratio, resulting in the compositions of quaternary $Co_{0.37}Ni_{0.26}Fe_{0.37}S_2$/ECT-$Co_{0.37}Ni_{0.26}Fe_{0.37}O$, as measured by inductively coupled plasma−mass spectrometry. This is probably due to the different electrodeposition kinetics and voltage required along with nickel, cobalt, and iron ions. Scanning transmission electron microscopy (STEM) and energy-dispersive X-ray spectroscopy (EDX) mapping of the quaternary $Co_{0.37}Ni_{0.26}Fe_{0.37}S_2$ were further employed to investigate the elemental distribution of the transition metal sulfides. The STEM image of $Co_{0.37}Ni_{0.26}Fe_{0.37}S_2$ shows the nanoporous characteristic of the nanosheets (Figure S5a), similar to that observed by SEM (Figure S4d). The STEM−EDX mapping of $Co_{0.37}Ni_{0.26}Fe_{0.37}S_2$ shows the even distribution of the elements of Co, Ni, Fe, and S on the porous nanosheets, demonstrating the uniform deposition of the sulfide nanosheets on the CFC.

We have also observed similar materials evolution in the ternary ECT-$Co_{0.5}Fe_{0.5}O$ and quaternary ECT-$Co_{0.37}Ni_{0.26}Fe_{0.37}O$. Owing to the robust in situ electrochemical oxidation tuning approach, the porous nanosheets of $Co_{0.37}Ni_{0.26}Fe_{0.37}S_2$ with high crystallinity (Figure S6a,b) were fully transferred to ECT-$Co_{0.37}Ni_{0.26}Fe_{0.37}O$ with smaller grain size nanoparticles and weak crystallinity (Figure S6d,e). The complete oxidation process was confirmed by the disappearance of S peak and the appearance of O peak in the EDX of ECT-$Co_{0.37}Ni_{0.26}Fe_{0.37}O$ (Figure S6f) with respect to that of $Co_{0.37}Ni_{0.26}Fe_{0.37}S_2$ (Figure S6c). The XRD further revealed the crystallinity and phase evolution of the ECT-$Co_{0.37}Ni_{0.26}Fe_{0.37}O$ (Figure S7), similar to that of the CoS_2/ECT-CoO system. This indicates that the in situ electrochemical tuning is a highly desirable and robust method for the tuning of different materials.

The electrocatalytic activity of our ECT-TMOs toward water oxidation was investigated in 1 M KOH electrolyte by the techniques of cyclic voltammetry (CV), electrochemical impedance spectroscopy (EIS), linear sweep voltammetry (LSV), and chronoamperometry (see Experimental Section in the Supporting Information for details). The catalytic activity of the pristine TMOs was also measured as control. The in situ electrochemical oxidation tuning process was conducted by CV scanning of TMSs in the electrolyte for a few cycles until stable curves were obtained. As shown in Figure 4a, the CoS_2 nanosheets underwent a very strong oxidation process at its first CV scan when they were tested under a moderate scan rate of 10 mV s^{-1} to a voltage of 1.2 V (vs SCE). The strong oxidation peak disappeared completely in the subsequent CV scans, indicating that the CoS_2 nanosheets have experienced a dramatic evolution and in situ oxidized in the first positive scan. The first irreversible CV scan was also observed in the ternary $Co_{0.5}Fe_{0.5}S_2$ and quaternary $Co_{0.37}Ni_{0.26}Fe_{0.37}S_2$ nanosheets (Figure 4a), implying that the in situ electrochemical oxidation tuning would be a general approach that is applicable to different sulfides. In contrast, such an in situ electrochemical oxidation process was not observed in the pristine TMOs, where the oxides show highly repeatable CV curves (Figure 4b). It is worth pointing out that the first in situ electrochemical oxidation process can be easily ignored if not enough attention was paid during the measurement. Interestingly, the in situ electrochemically tuned TMOs (ECT-TMOs) that derived from TMSs showed much more enhanced electrocatalytic activity toward water oxidation than that of the pristine TMOs in terms of overpotential, Tafel slope, and long-term cycling stability. As displayed in the polarization curves in Figure 4c and Figure S8, one can easily find that the TMOs exhibit much higher currents than that of the CFC substrate, suggesting that the major electrocatalytic contributions are from the TMOs and the negligible OER activity of the CFC. In addition, the OER activity can be enhanced by incorporation of Ni and Fe into the binary CoO, where the quaternary $Co_{0.37}Ni_{0.26}Fe_{0.37}O$/ECT-$Co_{0.37}Ni_{0.26}Fe_{0.37}O$ exhibit much lower overpotentials than that of the binary CoO/ECT-CoO and ternary $Co_{0.5}Fe_{0.5}O$/ECT-$Co_{0.5}Fe_{0.5}O$. The increased OER activity by the integration of Ni and/or Fe into CoO was consistent with the literature.[29,31,41] Moreover, the ECT-TMO electrodes are capable of delivering very high current densities (500−600 mA cm^{-2}) at higher overpotentials while keeping good linear polarization curves in the LSV measurements, demonstrating their outstanding performance that is highly desirable for practical application of the OER catalysts (Figure 4c). Most importantly, the OER activity of ECT-TMOs can be further greatly enhanced by the in situ electrochemical tuning, making the ECT-$Co_{0.37}Ni_{0.26}Fe_{0.37}O$ the best OER catalyst among all the investigated materials in this work. The anodic current density of the quaternary ECT-$Co_{0.37}Ni_{0.26}Fe_{0.37}O$ is much higher than that of the other materials at a certain potential, suggesting that much lower potential is required for ECT-$Co_{0.37}Ni_{0.26}Fe_{0.37}O$ to generate the same current. It was accepted to report the overpotentials of OER catalysts at a current density of 10 mA cm^{-2}, as it represents the upper limit of a device with 12% of solar to hydrogen efficiency.[33] As shown in Figure 4d and summarized in Table S1, the ECT-TMOs show lower overpotential than that of the pristine TMOs counterparts, confirming the efficacy of the in situ electrochemical tuning. The overpotential of the ECT-$Co_{0.37}Ni_{0.26}Fe_{0.37}O$ at a current density of 10 mA cm^{-2} is only 0.232 V, much lower than that of the pristine CoO (0.346 V), $Co_{0.5}Fe_{0.5}O$ (0.316 V), and $Co_{0.37}Ni_{0.26}Fe_{0.37}O$ (0.299 V), as well as ECT-CoO (0.284 V) and ECT-$Co_{0.5}Fe_{0.5}O$ (0.258 V). Surprisingly, the overpotential of the ECT-CoO at current density of 10 mA cm^{-2} (0.284 V) is even lower than that of the pristine $Co_{0.37}Ni_{0.26}Fe_{0.37}O$ (0.299 V), further highlighting the excellent capability of the in situ electrochemical tuning approach for enhanced water oxidation. Owning to the merits of the nanoporous nanosheets grown directly on the 3D electrodes, the nanostructured electrodes function to facilitate the release of the oxygen from the electrode surface and the evolved oxygen bubbles are accelerated by the available large surface area and efficient mass transportation. Therefore, high current densities can be achieved by the electrodes even at low overpotentials. For example, in order to generate a high current density of 500 mA cm^{-2}, the required overpotential for the pristine CoO is 514 mV, whereas it requires only 319 mV for

DOI: 10.1021/acscentsci.5b00227
ACS Cent. Sci. 2015, 1, 244−251

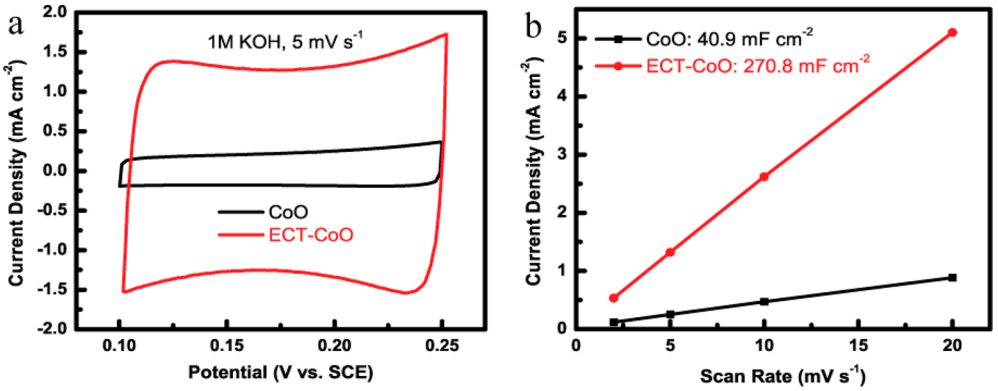

Figure 5. EDLC of the pristine CoO/ECT-CoO. (a) CV curves of the pristine CoO and ECT-CoO. (b) The current density at 0.2 V (vs SCE) with respect to scan rate for the pristine CoO and ECT-CoO.

the ECT-$Co_{0.37}Ni_{0.26}Fe_{0.37}O$ (Table S1). These values of the ECT-TMOs are among the best OER overpotentials based on different nonprecious catalysts reported so far (Table S2).[13−21,24]

The Tafel plots of the pristine TMOs and ECT-TMOs (Figure 4e) demonstrate distinct Tafel slopes which are summarized in Figure 4f and Table S1. Typically, nonprecious OER catalysts exhibit Tafel slopes in the range between 40 and 200 mV dec^{-1}. Our ECT-TMOs show the Tafel slopes ranging from 38 to 62 mV dec^{-1}, slightly lower than that of the pristine TMOs (Figure 4e,f). The incorporation of Ni and Fe into CoO effectively lowers the Tafel slopes (Figure 4f), suggesting the improved water oxidation reaction kinetics. Specifically, the quaternary ECT-$Co_{0.37}Ni_{0.26}Fe_{0.37}O$ (37.6 mV dec^{-1}) and the ternary ECT-$Co_{0.5}Fe_{0.5}O$ (38.9 mV dec^{-1}) show much lower Tafel slopes than that of the binary ECT-CoO (62.1 mV dec^{-1}), where the pristine TMOs followed a similar trend: $Co_{0.37}Ni_{0.26}Fe_{0.37}O$ (39.2 mV dec^{-1}) < $Co_{0.5}Fe_{0.5}O$ (41.7 mV dec^{-1}) < CoO (63.1 mV dec^{-1}). The small Tafel slopes observed in the ternary ECT-$Co_{0.5}Fe_{0.5}O$ (38.9 mV dec^{-1}) and quaternary ECT-$Co_{0.37}Ni_{0.26}Fe_{0.37}O$ (37.6 mV dec^{-1}) enable them to drive large current densities at low overpotentials, confirming the behaviors in the polarization curves (Figure 4c). Consistently, one noticeable characteristic of the ECT-TMOs is that the linear regions of the Tafel plots extend to high current densities (50−80 mA cm^{-2}, Figure 4e), indicating the excellent OER performance for the mass production of oxygen for practical applications. The possible effect of the capacitive/oxidation currents to the LSV and Tafel plot measurements can be eliminated by a reverse scan (from high to low overpotential) of the polarization curve (Figure S9). The results have been discussed and included in the Supporting Information, showing that the determination of the overpotentials at 10 mA cm^{-2} is very reasonable in this study. The most active OER catalyst in this work is the ECT-$Co_{0.37}Ni_{0.26}Fe_{0.37}O$, which has a very low overpotential of 232 mV at current density of 10 mA cm^{-2} and a small Tafel slope of 37.6 mV dec^{-1}. The excellent electrochemical performance of the ECT-$Co_{0.37}Ni_{0.26}Fe_{0.37}O$ is among one of the best reported OER catalysts based on different materials (Table S2).[28,33,36,38,41,52−55]

The catalytic stability is an important property metric for the realistic evaluation of the electrocatalysts. To investigate the stability of our ECT-TMOs, long-term electrolysis was carried out by chronopotentiometric measurement in 1 M KOH electrolyte at a constant current density of 20 mA cm^{-2}. Figure 4g shows that the ECT-TMOs retain excellent durability with high OER activities over the long-term electrolysis. Impressively, the quaternary ECT-$Co_{0.37}Ni_{0.26}Fe_{0.37}O$ catalyst exhibits exceptional durability with negligibly increased operation potential for over 100 h. As a result, the ECT-$Co_{0.37}Ni_{0.26}Fe_{0.37}O$ still maintained a low overpotential of 249 mV (corresponding to potential of 1.479 V vs RHE) after long-term electrolysis of 100 h at 20 mA cm^{-2}. The high Faradaic efficiency of our ECT-$Co_{0.37}Ni_{0.26}Fe_{0.37}O$ as very active OER catalyst is confirmed by gas chromatography measurement, as shown in Figure S10. In contrast, the catalysts of pristine CoO, $Co_{0.5}Fe_{0.5}O$, and $Co_{0.37}Ni_{0.26}Fe_{0.37}O$ showed higher overpotentials increase after even shorter terms of electrolysis. The outstanding long-term electrocatalytic stability of the ECT-TMOs with high OER activity demonstrates their promise as highly active and stable water oxidation catalysts.

In order to elucidate the much enhanced OER activity of the ECT-TMOs, we have conducted various characterizations on the analysis of materials evolution that were induced by the in situ electrochemical oxidation tuning and revealed the formation of nanopores accompanied by crystal phase evolution of the ECT-TMOs. We therefore expect an increase of surface area and active catalytic sites in the ECT-TMOs. As a proof of this claim, we have conducted electrochemical double layer capacitance (EDLC) measurements (a method that can be used to estimate the magnitude of electroactive surface area of electrode by the measurement of its capacitance) of the ECT-TMOs and compared them to the pristine TMOs (Figure S11−13). The ECT-CoO shows a much more increased cyclic voltammetry area than that of the pristine CoO at the same scan rate of 5 mV s^{-1}, indicating the much more enhanced surface area of the ECT-CoO (Figure 5a). As a result, the ECT-CoO shows a significantly enhanced areal capacitance of 270.8 mF cm^{-2}, which is about 6−7-fold higher than that of the pristine CoO (40.9 mF cm^{-2}) (Figure 5b). Figures S12 and S13 show the EDLC results of the ternary and quaternary TMOs and ECT-TMOs, respectively. The ternary ECT-$Co_{0.5}Fe_{0.5}O$ and quaternary ECT-$Co_{0.37}Ni_{0.26}Fe_{0.37}O$ also exhibit much more enhanced surface areas than those of their pristine TMOs. Specifically, the ECT-$Co_{0.5}Fe_{0.5}O$ shows a 2-fold active surface area increase over that of the pristine $Co_{0.5}Fe_{0.5}O$ (Figure S11). The ECT-$Co_{0.37}Ni_{0.26}Fe_{0.37}O$ demonstrates an enhanced areal capacitance of 296 mF cm^{-2}, which is about 6-fold higher than that of the pristine $Co_{0.37}Ni_{0.26}Fe_{0.37}O$ (50.5 mF cm^{-2}; Figure S12). The incorporation of nickel and iron into CoO/ECT-CoO leads to limited increase of the surface area, indicating

DOI: 10.1021/acscentsci.5b00227
ACS Cent. Sci. 2015, 1, 244−251

that the increased electrocatalytic activity of the mixed metal oxides is partially due to the synergistic effect of cobalt, nickel, and iron to the enhanced water oxidation.[30,50] Therefore, the in situ electrochemical oxidation tuning contributes to the significantly enhanced surface area and electrochemically active sites of the ECT-TMOs for largely improved OER activity. Overall, the drastic distinctions in terms of material crystallinity, composition, defects, grain boundaries, porosity, and active surface area are attributed to the in situ electrochemical oxidation tuning that stimulates the much enhanced water oxidation performance.

In conclusion, we have successfully developed a novel and facile in situ electrochemical oxidation tuning approach to synthesize various transition metal oxides with desirable characteristics as highly active catalysts for enhanced water oxidation. The in situ electrochemical tuning of transition metal sulfides gives rise to nanoporous oxides with much enhanced surface area and electroactive sites to drive significantly improved OER activity. The most active ECT-$Co_{0.37}Ni_{0.26}Fe_{0.37}O$ demonstrates a very low overpotential of 232 mV at current density of 10 mA cm^{-2}, a small Tafel slope of 37.6 mV dec^{-1}, and outstanding durability for over 100 h of long-term electrolysis and outperforms most of the nonprecious catalysts. In addition, the materials evolution associated with the in situ electrochemical tuning was systematically investigated by various characterizations. This work provides a promising approach to the development of highly efficient OER catalysts for water splitting devices and metal−air batteries.

■ ASSOCIATED CONTENT

Supporting Information

The following file is available free of charge on the ACS Publications website at DOI: 10.1021/acscentsci.5b00227.

Complete experimental details, additional characterization, and OER performance (PDF)

■ AUTHOR INFORMATION

Corresponding Author

*E-mail: yicui@stanford.edu.

Notes

The authors declare no competing financial interest.

■ ACKNOWLEDGMENTS

This work was initiated by the support of the Department of Energy, Office of Basic Energy Sciences, Materials Sciences and Engineering Division, under Contract DE-AC02-76-SFO0515. We acknowledge the support from Global Climate and Energy Projects (GCEP) at Stanford University.

■ REFERENCES

(1) Walter, M. G.; Warren, E. L.; McKone, J. R.; Boettcher, S. W.; Mi, Q.; Santori, E. A.; Lewis, N. S. Solar Water Splitting Cells. *Chem. Rev.* **2010**, *110*, 6446−6473.

(2) Tarascon, J. M.; Armand, M. Issues and challenges facing rechargeable lithium batteries. *Nature* **2001**, *414*, 359−367.

(3) Gratzel, M. Photoelectrochemical cells. *Nature* **2001**, *414*, 338−344.

(4) Gray, H. B. Powering the planet with solar fuel. *Nat. Chem.* **2009**, *1*, 7−7.

(5) Cheng, F.; Chen, J. Metal-air batteries: from oxygen reduction electrochemistry to cathode catalysts. *Chem. Soc. Rev.* **2012**, *41*, 2172−2192.

(6) Steele, B. C. H.; Heinzel, A. Materials for fuel-cell technologies. *Nature* **2001**, *414*, 345−352.

(7) Dresselhaus, M. S.; Thomas, I. L. Alternative energy technologies. *Nature* **2001**, *414*, 332−337.

(8) Subbaraman, R.; Tripkovic, D.; Chang, K. C.; Strmcnik, D.; Paulikas, A. P.; Hirunsit, P.; Chan, M.; Greeley, J.; Stamenkovic, V.; Markovic, N. M. Trends in activity for the water electrolyser reactions on 3d M(Ni,Co,Fe,Mn) hydr(oxy)oxide catalysts. *Nat. Mater.* **2012**, *11*, 550−557.

(9) Liang, Y.; Li, Y.; Wang, H.; Dai, H. Strongly Coupled Inorganic/Nanocarbon Hybrid Materials for Advanced Electrocatalysis. *J. Am. Chem. Soc.* **2013**, *135*, 2013−2036.

(10) Fang, Y.-H.; Liu, Z.-P. Mechanism and Tafel Lines of Electro-Oxidation of Water to Oxygen on RuO2(110). *J. Am. Chem. Soc.* **2010**, *132*, 18214−18222.

(11) Lee, Y.; Suntivich, J.; May, K. J.; Perry, E. E.; Shao-Horn, Y. Synthesis and Activities of Rutile IrO2 and RuO2 Nanoparticles for Oxygen Evolution in Acid and Alkaline Solutions. *J. Phys. Chem. Lett.* **2012**, *3*, 399−404.

(12) Gorlin, Y.; Jaramillo, T. F. A Bifunctional Nonprecious Metal Catalyst for Oxygen Reduction and Water Oxidation. *J. Am. Chem. Soc.* **2010**, *132*, 13612−13614.

(13) Tueysuez, H.; Hwang, Y. J.; Khan, S. B.; Asiri, A. M.; Yang, P. Mesoporous Co3O4 as an electrocatalyst for water oxidation. *Nano Res.* **2013**, *6*, 47−54.

(14) Liang, Y.; Li, Y.; Wang, H.; Zhou, J.; Wang, J.; Regier, T.; Dai, H. Co3O4 nanocrystals on graphene as a synergistic catalyst for oxygen reduction reaction. *Nat. Mater.* **2011**, *10*, 780−786.

(15) Gao, M.; Sheng, W.; Zhuang, Z.; Fang, Q.; Gu, S.; Jiang, J.; Yan, Y. Efficient Water Oxidation Using Nanostructured α-Nickel-Hydroxide as an Electrocatalyst. *J. Am. Chem. Soc.* **2014**, *136*, 7077−7084.

(16) Liu, Q.; Jin, J.; Zhang, J. NiCo2S4@graphene as a Bifunctional Electrocatalyst for Oxygen Reduction and Evolution Reactions. *ACS Appl. Mater. Interfaces* **2013**, *5*, 5002−5008.

(17) Zhao, W.; Zhang, C.; Geng, F.; Zhuo, S.; Zhang, B. Nanoporous Hollow Transition Metal Chalcogenide Nanosheets Synthesized via the Anion-Exchange Reaction of Metal Hydroxides with Chalcogenide Ions. *ACS Nano* **2014**, *8*, 10909−10919.

(18) Gao, M.-R.; Xu, Y.-F.; Jiang, J.; Zheng, Y.-R.; Yu, S.-H. Water Oxidation Electrocatalyzed by an Efficient Mn3O4/CoSe2 Nanocomposite. *J. Am. Chem. Soc.* **2012**, *134*, 2930−2933.

(19) Liu, Y.; Cheng, H.; Lyu, M.; Fan, S.; Liu, Q.; Zhang, W.; Zhi, Y.; Wang, C.; Xiao, C.; Wei, S.; Ye, B.; Xie, Y. Low Overpotential in Vacancy-Rich Ultrathin CoSe2 Nanosheets for Water Oxidation. *J. Am. Chem. Soc.* **2014**, *136*, 15670−15675.

(20) Gao, M.-R.; Cao, X.; Gao, Q.; Xu, Y.-F.; Zheng, Y.-R.; Jiang, J.; Yu, S.-H. Nitrogen-Doped Graphene Supported CoSe2 Nanobelt Composite Catalyst for Efficient Water Oxidation. *ACS Nano* **2014**, *8*, 3970−3978.

(21) Zheng, Y.-R.; Gao, M.-R.; Gao, Q.; Li, H.-H.; Xu, J.; Wu, Z.-Y.; Yu, S.-H. An Efficient CeO2/CoSe2 Nanobelt Composite for Electrochemical Water Oxidation. *Small* **2015**, *11*, 182−188.

(22) Kanan, M. W.; Nocera, D. G. In situ formation of an oxygen-evolving catalyst in neutral water containing phosphate and Co2+. *Science* **2008**, *321*, 1072−1075.

(23) Surendranath, Y.; Kanan, M. W.; Nocera, D. G. Mechanistic Studies of the Oxygen Evolution Reaction by a Cobalt-Phosphate Catalyst at Neutral pH. *J. Am. Chem. Soc.* **2010**, *132*, 16501−16509.

(24) Suntivich, J.; May, K. J.; Gasteiger, H. A.; Goodenough, J. B.; Shao-Horn, Y. A Perovskite Oxide Optimized for Oxygen Evolution Catalysis from Molecular Orbital Principles. *Science* **2011**, *334*, 1383−1385.

(25) Kim, J.; Yin, X.; Tsao, K.-C.; Fang, S.; Yang, H. Ca2Mn2O5 as Oxygen-Deficient Perovskite Electrocatalyst for Oxygen Evolution Reaction. *J. Am. Chem. Soc.* **2014**, *136*, 14646−14649.

(26) Long, X.; Li, J. K.; Xiao, S.; Yan, K. Y.; Wang, Z. L.; Chen, H. N.; Yang, S. H. A Strongly Coupled Graphene and FeNi Double

DOI: 10.1021/acscentsci.5b00227
ACS Cent. Sci. 2015, 1, 244−251

Hydroxide Hybrid as an Excellent Electrocatalyst for the Oxygen Evolution Reaction. *Angew. Chem., Int. Ed.* **2014**, *53*, 7584−7588.
(27) Trotochaud, L.; Ranney, J. K.; Williams, K. N.; Boettcher, S. W. Solution-Cast Metal Oxide Thin Film Electrocatalysts for Oxygen Evolution. *J. Am. Chem. Soc.* **2012**, *134*, 17253−17261.
(28) Gong, M.; Li, Y.; Wang, H.; Liang, Y.; Wu, J. Z.; Zhou, J.; Wang, J.; Regier, T.; Wei, F.; Dai, H. An Advanced Ni-Fe Layered Double Hydroxide Electrocatalyst for Water Oxidation. *J. Am. Chem. Soc.* **2013**, *135*, 8452−8455.
(29) McCrory, C. C. L.; Jung, S. H.; Peters, J. C.; Jaramillo, T. F. Benchmarking Heterogeneous Electrocatalysts for the Oxygen Evolution Reaction. *J. Am. Chem. Soc.* **2013**, *135*, 16977−16987.
(30) Hunter, B. M.; Blakemore, J. D.; Deimund, M.; Gray, H. B.; Winkler, J. R.; Mueller, A. M. Highly Active Mixed-Metal Nanosheet Water Oxidation Catalysts Made by Pulsed-Laser Ablation in Liquids. *J. Am. Chem. Soc.* **2014**, *136*, 13118−13121.
(31) Burke, M. S.; Kast, M. G.; Trotochaud, L.; Smith, A. M.; Boettcher, S. W. Cobalt-Iron (Oxy)hydroxide Oxygen Evolution Electrocatalysts: The Role of Structure and Composition on Activity, Stability, and Mechanism. *J. Am. Chem. Soc.* **2015**, *137*, 3638−3648.
(32) Louie, M. W.; Bell, A. T. An Investigation of Thin-Film Ni-Fe Oxide Catalysts for the Electrochemical Evolution of Oxygen. *J. Am. Chem. Soc.* **2013**, *135*, 12329−12337.
(33) Song, F.; Hu, X. L. Exfoliation of layered double hydroxides for enhanced oxygen evolution catalysis. *Nat. Commun.* **2014**, DOI: 10.1038/ncomms5477.
(34) Fominykh, K.; Feckl, J. M.; Sicklinger, J.; Doeblinger, M.; Boecklein, S.; Ziegler, J.; Peter, L.; Rathousky, J.; Scheidt, E.-W.; Bein, T.; Fattakhova-Rohlfing, D. Ultrasmall Dispersible Crystalline Nickel Oxide Nanoparticles as High-Performance Catalysts for Electrochemical Water Splitting. *Adv. Funct. Mater.* **2014**, *24*, 3123−3129.
(35) Dinca, M.; Surendranath, Y.; Nocera, D. G. Nickel-borate oxygen-evolving catalyst that functions under benign conditions. *Proc. Natl. Acad. Sci. U. S. A.* **2010**, *107*, 10337−10341.
(36) Smith, R. D. L.; Prevot, M. S.; Fagan, R. D.; Zhang, Z.; Sedach, P. A.; Siu, M. K. J.; Trudel, S.; Berlinguette, C. P. Photochemical Route for Accessing Amorphous Metal Oxide Materials for Water Oxidation Catalysis. *Science* **2013**, *340*, 60−63.
(37) Indra, A.; Menezes, P. W.; Sahraie, N. R.; Bergmann, A.; Das, C.; Tallarida, M.; Schmeisser, D.; Strasser, P.; Driess, M. Unification of Catalytic Water Oxidation and Oxygen Reduction Reactions: Amorphous Beat Crystalline Cobalt Iron Oxides. *J. Am. Chem. Soc.* **2014**, *136*, 17530−17536.
(38) Smith, R. D. L.; Prevot, M. S.; Fagan, R. D.; Trudel, S.; Berlinguette, C. P. Water Oxidation Catalysis: Electrocatalytic Response to Metal Stoichiometry in Amorphous Metal Oxide Films Containing Iron, Cobalt, and Nickel. *J. Am. Chem. Soc.* **2013**, *135*, 11580−11586.
(39) Wang, H.; Lu, Z.; Xu, S.; Kong, D.; Cha, J. J.; Zheng, G.; Hsu, P.-C.; Yan, K.; Bradshaw, D.; Prinz, F. B.; Cui, Y. Electrochemical tuning of vertically aligned MoS2 nanofilms and its application in improving hydrogen evolution reaction. *Proc. Natl. Acad. Sci. U. S. A.* **2013**, *110*, 19701−19706.
(40) Wang, H.; Lu, Z.; Kong, D.; Sun, J.; Hymel, T. M.; Cui, Y. Electrochemical Tuning of MoS2 Nanoparticles on Three-Dimensional Substrate for Efficient Hydrogen Evolution. *ACS Nano* **2014**, *8*, 4940−4947.
(41) Lu, Z. Y.; Wang, H. T.; Kong, D. S.; Yan, K.; Hsu, P. C.; Zheng, G. Y.; Yao, H. B.; Liang, Z.; Sun, X. M.; Cui, Y. Electrochemical tuning of layered lithium transition metal oxides for improvement of oxygen evolution reaction. *Nat. Commun.* **2014**, DOI: 10.1038/ncomms5345.
(42) Liu, Y.; Wang, H.; Lin, D.; Liu, C.; Hsu, P.-C.; Liu, W.; Chen, W.; Cui, Y. Electrochemical tuning of olivine-type lithium transition-metal phosphates as efficient water oxidation catalysts. *Energy Environ. Sci.* **2015**, *8*, 1719.
(43) Wang, H.; Lee, H.-W.; Deng, Y.; Lu, Z.; Hsu, P.-C.; Liu, Y.; Lin, D.; Cui, Y. Bifunctional non-noble metal oxide nanoparticle electrocatalysts through lithium-induced conversion for overall water splitting. *Nat. Commun.* **2015**, DOI: 10.1038/ncomms8261.
(44) Lin, J. Y.; Liao, J. H. Mesoporous Electrodeposited-CoS Film as a Counter Electrode Catalyst in Dye-Sensitized Solar. *J. Electrochem. Soc.* **2012**, *159*, D65−D71.
(45) Chen, W.; Xia, C.; Alshareef, H. N. One-Step Electrodeposited Nickel Cobalt Sulfide Nanosheet Arrays for High-Performance Asymmetric Supercapacitors. *ACS Nano* **2014**, *8*, 9531−9541.
(46) Legrand, D. L.; Nesbitt, H. W.; Bancroft, G. M. X-ray photoelectron spectroscopic study of a pristine millerite (NiS) surface and the effect of air and water oxidation. *Am. Mineral.* **1998**, *83*, 1256−1265.
(47) Yang, J.; Liu, H.; Martens, W. N.; Frost, R. L. Synthesis and Characterization of Cobalt Hydroxide, Cobalt Oxyhydroxide, and Cobalt Oxide Nanodiscs. *J. Phys. Chem. C* **2010**, *114*, 111−119.
(48) Kung, C.-W.; Chen, H.-W.; Lin, C.-Y.; Huang, K.-C.; Vittal, R.; Ho, K.-C. CoS Acicular Nanorod Arrays for the Counter Electrode of an Efficient Dye-Sensitized Solar Cell. *ACS Nano* **2012**, *6*, 7016−7025.
(49) McAlpin, J. G.; Surendranath, Y.; Dinca, M.; Stich, T. A.; Stoian, S. A.; Casey, W. H.; Nocera, D. G.; Britt, R. D. EPR Evidence for Co(IV) Species Produced During Water Oxidation at Neutral pH. *J. Am. Chem. Soc.* **2010**, *132*, 6882−6883.
(50) Gerken, J. B.; Shaner, S. E.; Masse, R. C.; Porubsky, N. J.; Stahl, S. S. A survey of diverse earth abundant oxygen evolution electrocatalysts showing enhanced activity from Ni-Fe oxides containing a third metal. *Energy Environ. Sci.* **2014**, *7*, 2376−2382.
(51) Yuan, C.; Li, J.; Hou, L.; Zhang, X.; Shen, L.; Lou, X. W. Ultrathin Mesoporous NiCo2O4 Nanosheets Supported on Ni Foam as Advanced Electrodes for Supercapacitors. *Adv. Funct. Mater.* **2012**, *22*, 4592−4597.
(52) Hunter, B. M.; Blakemore, J. D.; Deimund, M.; Gray, H. B.; Winkler, J. R.; Müller, A. M. Highly Active Mixed-Metal Nanosheet Water Oxidation Catalysts Made by Pulsed-Laser Ablation in Liquids. *J. Am. Chem. Soc.* **2014**, *136*, 13118−13121.
(53) Luo, J.; Im, J.-H.; Mayer, M. T.; Schreier, M.; Nazeeruddin, M. K.; Park, N.-G.; Tilley, S. D.; Fan, H. J.; Gratzel, M. Water photolysis at 12.3% efficiency via perovskite photovoltaics and Earth-abundant catalysts. *Science* **2014**, *345*, 1593−1596.
(54) Zhao, A.; Masa, J.; Xia, W.; Maljusch, A.; Willinger, M.-G.; Clavel, G.; Xie, K.; Schlögl, R.; Schuhmann, W.; Muhler, M. Spinel Mn−Co Oxide in N-Doped Carbon Nanotubes as a Bifunctional Electrocatalyst Synthesized by Oxidative Cutting. *J. Am. Chem. Soc.* **2014**, *136*, 7551−7554.
(55) Song, F.; Hu, X. Ultrathin Cobalt−Manganese Layered Double Hydroxide Is an Efficient Oxygen Evolution Catalyst. *J. Am. Chem. Soc.* **2014**, *136*, 16481−16484.

DOI: 10.1021/acscentsci.5b00227
ACS Cent. Sci. 2015, 1, 244−251